1 Introduction

Polymer foams are an aspect of modern life. Disposable packaging of fast food, building insulation, cushioning of furniture, running shoes and bicycle helmets are a few examples [1]. The properties of the foams differ considerably with the polymer and its processing. While polystyrene (PS) is a common example for insulation applications, polymethylmethacrylate (PMMA) is often used in automotive industry and civil engineering because of its exceptional resistance to weathering [2].

In recent years the prospect of foams with a pore size in the submicron range has achieved increasing attention. These materials exhibit a high application and market potential due to a high-performance thermal insulation capacity which can be improved by a factor of at least 3 if the pores are smaller than 100 nm [3]. A high sound absorption, optical transparency and a uniquely high stability against applied forces are further benefits [4, 5]. The reasons for these improved features are based on the nanostructure. Optical transparency is achieved because light scattering is negligible if the pore size is much smaller than the wavelength of visible light. The Knudsen effect predicts that heat transfer over the cell gas collapses if the pore size of the foam pore which encloses the gas is smaller than the mean free path length of the gas [6-8], explaining the improvement of heat insulation. This is valid for foams with pore sizes smaller than 100 nm [9].

Motivated by these promising characteristics different approaches to nanoporous materials were developed. To date, the only nano-porous bulk materials realised are aerogels [4]. They can consist of organic, inorganic or organic-inorganic hybrid networks which form a highly porous solid material [4, 10-13]. Preparation of aerogels according to the sol-gel-process invented by Kistler [14, 15] starts from a precursor substance dissolved in an adequate solvent. The addition of a catalyst induces formation of sol particles with a size of a few nanometres. These particles aggregate to a network structure which builds the foundation of the future aerogel. The solvent removal, i.e. drying, further shrinks the characteristic size of the solid aerogel by about two orders of magnitude. In order to keep the network structure intact the use of supercritical fluids is necessary. These enable a continuous and steady process without many capillary forces if the pressure and thus the density of the supercritical fluid is reduced carefully. This process is gentle but slow which makes aerogels expensive and limits their use to special applications like space engineering [16, 17].

A promising two-step process to nano-porous foams was presented in 1987 by Colton and Suh [18-22]. The first step consists of the saturation of a glassy thermoplastic polymer with an inert blowing agent like CO_2 which diffuses into the polymer. In a second step the temperature is raised above the glass transition temperature T_G. Releasing the pressure leads to a foaming due to the blowing agent inside the polymer. Thereby, the morphology of the resulting material depends on saturation pressure, foaming time and temperature. This concept was successfully applied by Krause *et al.* to, for example, polyetherimides, resulting in foams with an open cell porosity down to 100 nm [23-27]. Since,

1

however, already thin films of a few millimetres require saturation times of several hours this technique is not appropriate for bulk materials.

Another approach to nanoporous materials was developed by Strey and Müller in 2011 [28, 29]. The "Nano-Foams by Continuity Inversion of Dispersion" (NF-CID) principle utilises the voids in a close-packed colloidal polymer nano-lattice. They are filled with super- or near-critical fluid at appropriate pressure and at a temperature below T_G. Since the filling is not diffusion-limited it is finished within seconds. The lower interfacial tension of polymer and fluid compared to the higher polymer-air interfacial tension further promotes this process. Traversing T_G, which is lowered by the presence of supercritical fluids like CO_2 [30], induces a "continuity inversion". Now, the former discrete polymer particles melt into one continuous material in which the former voids develop nano-sized spherical inclusions. Diameter and number density of the inclusions are directly proportional to the size of the polymer particles. Releasing the pressure leads to a foaming of the material and a simultaneous fixation of the foam due to an increase of T_G. Compared to the procedure by Krause *et al.* the important advantage of the NF-CID principle is that no saturation times are necessary, resulting in considerably lower preparation times. Applying this procedure PS as well as PMMA foams with pore diameters in the submicron range were realised [29].

The "Principle of Supercritical Microemulsion Expansion" (POSME) [31, 32] was presented by Schwan, Sottmann and Strey in 2003. Here, thermodynamically stable, nanostructured microemulsions are used as a template. In microemulsions an amphiphilic surfactant film mediates the mixture of two otherwise immiscible components by separating them on the nanoscale. The driving force behind that process is the dramatically decreased interfacial tension. The POSME procedure suggests the use of compressed near- or supercritical fluids which function as hydrophobic component and simultaneously as blowing agent. Thereby, a detailed knowledge of phase behaviour and microstructure of supercritical microemulsions [33-40] is crucial. Fixation, i.e. polymerisation [41-44], and expansion, i.e. an increase of volume, are known to induce demixing process. These are accompanied by coarsening like Ostwald ripening [45] and coagulation with subsequent coalescence [46]. POSME foams display pore sizes in the range of 100 µm [29, 47, 48].

In order to prevent or slow down ageing processes the concept of "Anti-Ageing Agents (AAA) for Nanoporous foams" was developed by Strey *et al.* [47, 49]. This concept is based on the addition of a low-molecular hydrophobic additive to supercritical microemulsions. It is supposed to accumulate at the thermodynamically unfavourable contact sites of CO_2 and the polar component, lowering the interfacial tension. These contact sites emerge due to an increase of volume upon expansion. The influence of the cyclohexane mass fraction in the hydrophobic phase $\beta_{cyclohexane}$ on balanced microemulsions of the type brine – CO_2 – fluorinated surfactants has been systematically studied previously as shown in Figure 1.1 left. Note that the efficiency of the system without cyclohexane, i.e. at $\beta_{cyclohexane} = 0.0$, strongly depends on pressure. The weight mass fraction $\tilde{\gamma}$ needed to formulate a

2

one-phase microemulsion can be considerably reduced by increasing the pressure from 150 to 300 bar. This is due to an increase of density of CO_2 which leads to a reduced interfacial tension with water [50, 51] and an improved surface-to-volume ratio.
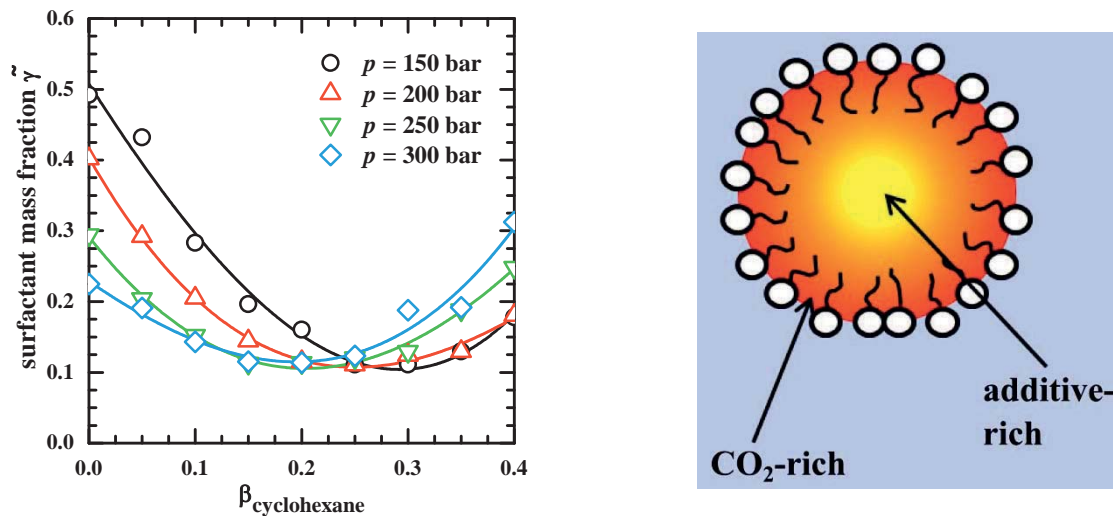

Figure 1.1: *Left:* Plot of the surfactant mass fraction $\tilde{\gamma}$ at the point of maximum efficiency against the mass fraction $\beta_{cyclohexane}$ of cyclohexane in the hydrophobic phase, for the balanced microemulsion system H_2O/NaCl – CO_2/ cyclohexane – Zonyl FSO 100/ Zonyl FSN 100 ($\alpha = 0.4$, $\delta_{FSN} = 0.75$, $\varepsilon = 0.01$). The efficiency increases to a pressure-specific cyclohexane mass fraction but decreases if this concentration is exceeded [52, 53]. *Right:* Graphic illustration of the hypothesis of a concentration gradient of cyclohexane in a micelle with fluorinated surfactants. Taken from [52].

Surprisingly, it was found that the partial replacement of CO_2 by cyclohexane enables a reduction of fluorinated surfactant by a factor 2 at $p = 300$ bar and even 5 at $p = 150$ bar. Here, the higher efficiency at $\beta_{cyclohexane} = 0.0$ and 300 bar offers less potential improvement than at 150 bar. The repulsive interactions between fluorinated surfactants and protonated substances such as cyclohexane [54, 55] likely reduce the monomeric solubility of fluorinated surfactants in the CO_2/cyclohexane mixture, which is rather high (11 wt%) in case of pure CO_2 [34]. However, the decreased monomeric solubility and hence increased interfacial area is not sufficient to explain the enormous and unexpected efficiency increase. Thus, a hypothesis to explain this effect was postulated [52] which is shown graphically in Figure 1.1 right. Based on the repulsive cyclohexane/ fluorinated surfactant tails interactions the formation of a depletion zone of cyclohexane close to the surfactants and a cyclohexane-enriched zone at the centre of the domains was postulated. This would result in a concentration gradient of cyclohexane within the respective microemulsion domains. The observed trend of $\tilde{\gamma}$ with β (Figure 1.1 left) might be discussed as follows: Increasing the mass fraction $\beta_{cyclohexane}$ of cyclohexane in the CO_2-swollen domains leads to the formation of a depletion zone, which becomes more and more pronounced and causes a considerable decrease of $\tilde{\gamma}$, i.e. an increase of efficiency. This may be caused by improved CO_2/ surfactant interactions triggered through repulsive interactions of cyclohexane and the fluorinated surfactant chains. Above a certain (pressure

3

dependent) concentration of cyclohexane, a spatially avoidance of repulsive interactions is no longer possible, causing a decrease of efficiency. At the outset of this work, however, this was only a postulation.

In the context of supercritical microemulsions the investigation of the kinetics of structural changes is a challenge which has so far only been met by Müller *et al.* [29, 56]. A high-pressure cell for small-angle neutron scattering (SANS) which provides stroboscopic pressure jumps with adjustable amplitude was developed by the mechanical workshop of the University of Cologne within the frame of the BMBF project TISANE [57, 58]. A schematic drawing of this cell is shown in Figure 1.2. Therein, the key component is a metal bellow (green) which is inserted into the sample volume (orange). By pumping hydraulic oil (yellow) in or out of the bellow it can extend or shrink, respectively, and thus transfer different pressures. Pressure jumps can be performed with a maximum frequency of 5 Hz (status as of March 2013) whereby the maximum pressure is 300 bar. Since the bellow provides nearly unlimited repeatability of pressure jumps this stroboscopic high-pressure SANS cell (SHP-SANS cell) is a unique setup.
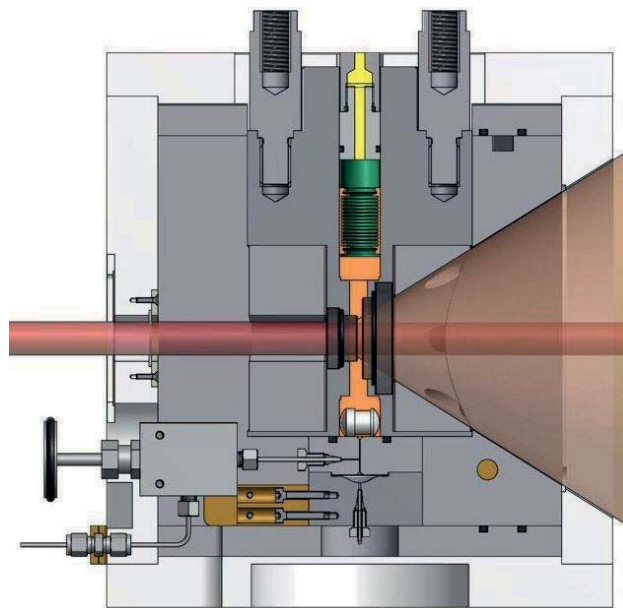

Figure 1.2: Cross section of the SHP-SANS cell, prepared by the internal mechanical workshop. The sample volume, which is sealed by two sapphire windows, is marked in orange, where the neutron beam (red) is partly scattered. The pressure jump is performed by means of a metal bellow (green) which can shrink or extend in order to transfer the desired pressure.

Using the SHP-SANS cell the demixing kinetics of a CO_2-microemulsion were investigated, showing that they strongly depend on the depth of the pressure jump [29]. In the frame of the anti-ageing project Müller also formulated a diluted microemulsion with 20 wt% cyclohexane in the mixture of cyclohexane and CO_2 and found an increase of microemulsion efficiency similar to the one described for balanced microemulsions (see Figure 1.1 left). The reason for this effect, however, was not yet explained. It turned out that the substitution of CO_2 by cyclohexane decelerates the demixing process

4

by one order of magnitude. The TISANE option itself, an instrumental setup to investigate kinetic processes with a time resolution < 5 ms, was not yet applied successfully in combination with the SHP-SANS cell. This is due to the fact that the achieved pressure jump frequency (5 Hz) was too slow for the TISANE requirements [29].

Kinetic processes, however, are also important in the area of biomedical applications. Here, understanding drug-release kinetics is of fundamental interest. In this field especially Poly-(*N*-isopropylacrylamide) (PNIPAM) microgel particles have attracted much attention in recent years. Their lower critical solution temperature is located around 32°C and therefore very close to the temperature of the human body [59-61]. At this temperature PNIPAM particles undergo a change from swollen microgel to dehydrated spheres due to a change of miscibility with the solvent [62-64]. Co-nonsolvency, which means that PNIPAM particles are soluble in two different solvents (such as water and methanol) but not necessarily in mixtures of both, has also been thoroughly investigated [65, 66]. Besides that other stimuli like pH, salt concentration, solvent composition and also the effect of hydrostatic pressure on the swelling behaviour of microgels were tested [67-69].

However, there are hardly any publications on the kinetics of the volume transition so far, which are crucial for biomedical applications. Admittedly, kinetics according to a change of temperature are difficult to determine. While a rapid heating of the particles can be performed applying for example a Joule-heating temperature jump [70], fast and precise cooling is a challenge. To date, such measurements were only possible by modifying the particles [71, 72]. Utilising small iron oxide particles at the PNIPAM surface rapid magnetic heating can be induced [73]. However, these techniques do not feature a fast repetition as the rebuilding of the initial structure, e.g. by external cooling, is slow. Using co-nonsolvency to induce the structural changes, for example in stopped-flow devices, allows a fast repetition of the experiment [74]. However, since the structural changes are induced by a change of composition the correlation to temperature-induced kinetics is vague.

Recently, it turned out that the transition temperature of thermoresponsive materials can be shifted to higher temperatures by hydrostatic pressure [29, 75]. Consequently, both swelling and deswelling kinetics can be investigated using the SHP-SANS cell. The benefit of hydrostatic pressure is that it can be changed rapidly and reversibly and occurs homogeneously throughout the sample without any gradients like in temperature-changing setups. Such measurements will provide completely new insights into the kinetics of structural changes of thermoresponsive polymers.

The intersection of these two soft-matter systems are consequently microemulsions with polymer particles in the hydrophilic phase. Comparable systems are known as orthogonal self-assembled systems, describing independently coexisting structures [76]. While the most obvious example for such systems are the complex mixtures of structures present in living cells, a variety of systematic studies on less complex systems exists [77-79]. Recently Laupheimer *et al.* identified a gelled bicontinuous microemulsion as an orthogonal self-assembled system and investigated its phase

5

behaviour and microstructure [80, 81]. Unifying articles on both microemulsions and polymer particles commonly deal with particle synthesis using either the high interfacial area or the nanostructure of microemulsions [82-86]. The only study concentrating on the coexistence of microemulsions and PNIPAM particles (Zhou and Wu, 1995) is on the influence of PNIPAM particles on water – hexane – SDS/AOT microemulsions, finding that PNIPAM acts as a stabiliser [87].

Here, the SHP-SANS cell enables not only a detailed investigation of such coexisting structures by means of SANS. It also permits studying the influence of polymer particles on the kinetics of pressure-induced structural changes on microemulsions. Applying appropriate contrast conditions this can also be studied vice versa.

OBJECTIVES

Cyclohexane was found to considerably increase the efficiency of balanced microemulsions of the type brine – CO_2 – fluorinated surfactants [29, 52] which is unexpected due to repulsive interactions of hydrophobic protonated and fluorinated substances. The hypothesis of a concentration gradient of cyclohexane with a depletion zone close to the amphiphilic film was postulated but not yet proven [52]. Thus, performing a systematic SANS contrast variation with subsequent detailed analysis of the scattering data was the first goal of this work. The *Generalised Indirect Fourier Transformation* was to be applied to elucidate the distribution of cyclohexane in such micelles.

Furthermore, a systematic study on the influence of cyclohexane on phase behaviour and microstructure of diluted microemulsions of the same type was planned. It was intended to systematically investigate pressure-induced elongation processes within the thermodynamically stable state at different cyclohexane concentrations. Furthermore, the demixing properties of microemulsions with different cyclohexane contents upon a pressure jump to 70 bar, at which a CO_2-in-water microemulsion coexists with a CO_2-excess phase, was to be examined.

Besides microemulsions the influence of hydrostatic pressure on different PNIPAM particles was to be studied. Using the SHP-SANS cell should also reveal kinetic aspects of pressure-induced structural changes at temperatures close to the volume phase transition temperature.

Since the focus was on both microemulsions and PNIPAM particles it reasonably follows to also investigate both systems under mutual confinement, i.e. study phase behaviour and microstructure. Again provided by means of the SHP-SANS cell first SANS experiments regarding kinetic processes under confinement of the respective structure were planned.

Since the SHP-SANS cell is the main tool of this work the improvement of this unique sample holder was an important aspect throughout this work. Especially regarding the possible application of the cell for TISANE measurements it was important to perform faster pressure jumps in order to meet the TISANE principle requirements.

6

2 Fundamentals

2.1 Microemulsions

The first time that a mixture of water – soap – oil was described in dependence of temperature and composition was by Schulman and Hoar in 1943 [88], although the term "microemulsion" was not used until 1959 [89]. Using ionic surfactants, Winsor performed a systematic study of the three-phase region with ionic surfactants [90] and classified four different phase equilibria [91]. The temperature sensitivity of the one-phase microemulsion with non-ionic surfactant was described 1967 by Shinoda [92-95]. Starting from there, the most significant work regarding phase behaviour and microstructure of microemulsions with non-ionic surfactant was performed by Kahlweit and co-workers [96, 97].

Microemulsions are by definition thermodynamically stable, macroscopically homogeneous and isotropic but nano-structured mixtures of at least three components [97-99]. Two of these three components are mutually immiscible, for example a polar one (water, A) and a hydrophobic one (alkane, B). The third, amphiphilic component (C), a surfactant, mediates the mixing by adsorbing at the interface between the immiscible components due to its amphiphilic nature and thus reducing the interfacial tension σ by several orders of magnitude. For the system water – octane σ is reduced from 50 mN m^{-1} [100] to $4.9 \cdot 10^{-3}$ mN m^{-1} upon addition of the surfactant $C_{10}E_5$ [101]. The amphiphilic nature of the surfactant is due to its ambivalent structure. It is composed of the hydrophilic head group which is soluble in polar substances and the hydrophobic tail which is soluble in non-polar oils. Surfactants can be non-ionic, cationic, anionic, zwitterionic or amphotheric depending on the nature of the polar head group. In this work, only non-ionic surfactants were used. Common commercially available non-ionic surfactants are *n*-alkyl-polyglycol ether which consist of a tail with *i* CH_2 units and have *j* glycol units in the polar head group. Thus, they are commonly abbreviated with C_iE_j.

Although macroscopically a microemulsion is isotropic and homogeneous, on a microscopic scale the two immiscible components are still separated from each other by an extended film of a monolayer of surfactant. Depending on parameters like composition, temperature and, in the case of compressible components, hydrostatic pressure one finds a number of different equilibrium states, and among these occur numerous different structures like spherical droplets or bicontinuous phases. In order to investigate kinetics of structural changes in microemulsions, it is crucial to understand the phase behaviour of microemulsions first.

2.1.1 Phase behaviour of binary mixtures

The binary systems water (A) – oil (B), water (A) – non-ionic surfactant (C) and oil (B) – non-ionic surfactant (C) display characteristic miscibility gaps depending on temperature and composition. A schematic drawing of these systems is shown in Figure 2.1. For the two immiscible components (A) and (B) the miscibility gap can be found over the whole temperature range with the critical point far

above the boiling point of the single components. In the mixture of the hydrophobic component and the non-ionic surfactant only a lower miscibility gap occurs, with an upper critical point cp_α with its corresponding temperature T_α which is usually below the freezing point of the mixture [102]. cp_α and T_α, however, depend strongly on the nature of the surfactant.

The mixture (A) – (C) also has a lower miscibility gap which is usually well below the melting point of the mixture, and is therefore difficult to measure. More important for microemulsions is the upper miscibility gap which is closed for thermodynamic reasons. Consequently, there is an upper and a lower critical point. The upper critical point usually lies above the boiling point and is therefore not of interest for the phase behaviour of microemulsions. The lower critical point cp_β, however, is normally in a temperature range which is relevant to microemulsions. The location of this miscibility gap depends on the amphiphilic features of the surfactant and the composition of the polar phase. Between the upper and the lower miscibility gap the surfactant is monomerically dissolved in the polar phase at very low surfactant concentrations. Increasing the surfactant concentration leads to surfactant micelles above the critical micelle concentration (*cmc*) [103]. If the surfactant concentration is increased further, lyotropic mesophases (´liquid crystals´) occur with almost all types of amphiphiles [104].
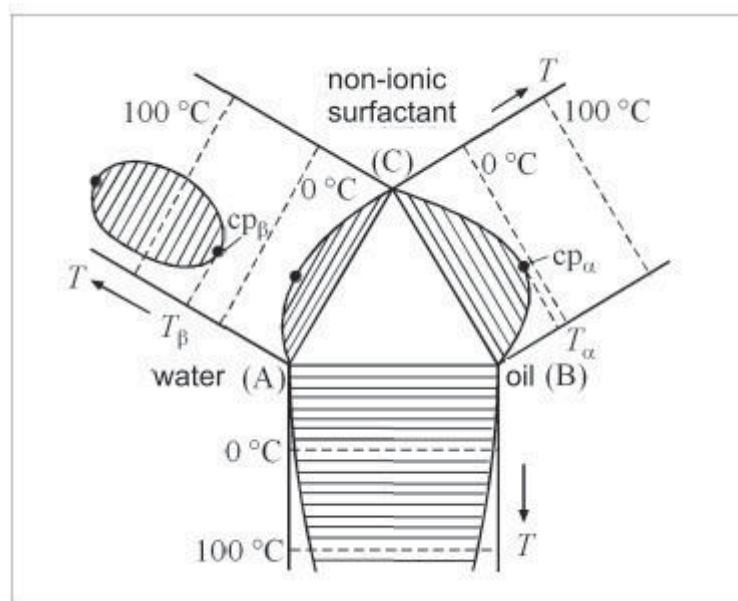

Figure 2.1: Schematic drawing of the three binary systems (A)-(B), (A)-(C) and (B)-(C). While (A) and (B) are immiscible over almost the whole temperature range, B and C only have a lower miscibility gap which is often below 0°C. (A) and (C) show a lower miscibility gap, which is lower than the miscibility gap of the system (B)-(C) , and an upper miscibility gap which is relevant to microemulsions. Redrawn from [97].

2.1.2   The phase prism – ternary mixtures

Starting from the triangle shown in Figure 2.2 with the three components at the edges and using the temperature as the ordinate perpendicular to this base triangle, i.e. flipping up the side systems, the Gibbs phase prism is generated. At ternary mixtures, i.e. at compositions between the binary systems

8

at the sides of the prism, many different phases can be observed. The phase behaviour is quite complex and mainly depends on the interplay of the upper miscibility gap of water and non-ionic surfactant and the lower miscibility gap of oil and non-ionic surfactant. Furthermore, the change of solubility of the surfactant from soluble in water at low temperature to soluble in oil at high temperature is a determining factor. This change of solubility can be explained by the partial dehydration of the surfactant head group at high temperature [105].
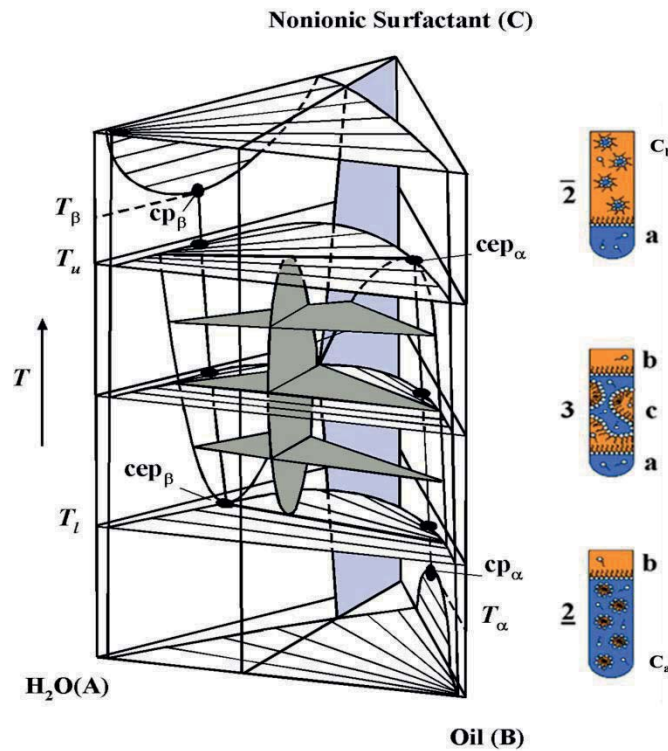

Figure 2.2: Schematic phase prism of a ternary mixture containing water (A), oil (B) and non-ionic surfactant (C). Highlighted in grey is the three-phase region, in light blue the one-phase region. The test tubes on the right illustrate the different states of $\underline{2}$, 3 and $\overline{2}$. Redrawn from [106].

The test tubes shown in Figure 2.2 next to the phase prism indicate different possible equilibrium states of the mixture at three different temperatures. Starting at low temperatures, a surfactant-rich oil-in-water (o/w)-microemulsion (c_a) coexists with an oil excess phase (b) (lowest test tube). Surfactant molecules are monomerically dissolved in both phases. Since the interactions between water and surfactant are much stronger than the ones between surfactant and oil, the amphiphilic film is curved around the oil. The surfactant-rich microemulsion phase is usually of higher density, so that it is below the oil excess phase. This state is termed $\underline{2}$ to indicate that the lower phase is the surfactant-rich microemulsion.

By increasing the temperature (middle test tube) the interactions of surfactant and polar phase are weakened, which leads to a partial dehydration of the polar head groups of the surfactant. This lowers the solubility of surfactant in the polar phase, until at the temperature T_l the oil-in-water microemulsion splits up to a surfactant-rich microemulsion (c_a) and a water excess phase (a) because

9

the surfactant interacts about equally well with water and oil. The volume of the oil excess phase (b) decreases because more oil can be dissolved in the microemulsion phase (c), which in turn grows in volume. Therefore, three phases coexist at ambient temperatures. Because the surfactant interacts well both with water and oil at ambient temperature the curvature of the microemulsion phase (c) is zero.

By increasing the temperature further (upper test tube) the hydrophobic interactions of surfactant and oil become stronger, and thus the microemulsion phase dissolves more oil until at a certain temperature T_u the microemulsion phase (c) merges with the oil excess phase (b) to a surfactant-rich water-in-oil (w/o)-microemulsion (c_b) and a water excess phase (a). As the density of the microemulsion is now usually lower than the one of the water excess phase, the surfactant-rich microemulsion is the upper phase, which is indicated by $\overline{2}$.

The determination of all phase boundaries in a three-dimensional Gibbs phase prism is complicated and a lot of work. Therefore, it is convenient to use different sections through the phase prim by keeping one ratio constant [99]. Examples are the $T(\gamma)$ section and the $T(w_B)$-section which are both shown schematically in Figure 2.3.
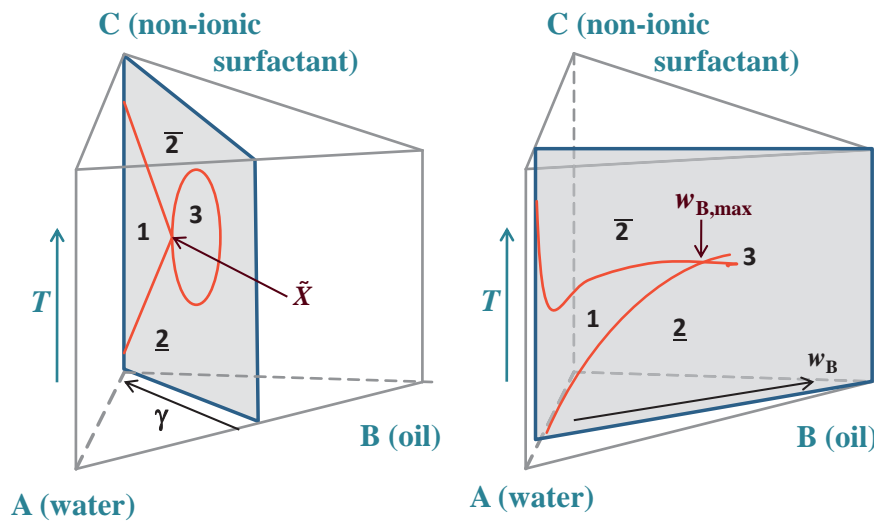

Figure 2.3: $T(\gamma)$-section (left) and $T(w_B)$-section (right) through the upright phase prism. The $T(\gamma)$-section shows a variation of temperature and surfactant mass fraction γ at a constant water-to-oil ratio, whereas the water-surfactant ratio is kept constant in a $T(w_B)$-section. Here, the oil mass fraction w_B is varied.

Figure 2.3 left shows a schematic drawing of a $T(\gamma)$-section [97, 107]. Here, ratio alpha

$$\alpha = \frac{m_B}{m_A + m_B} \qquad \text{Eq. 2-1}$$

of oil in the mixture of water and oil is kept constant and the surfactant concentration γ is varied, with γ being the mass fraction of surfactant in the overall mixture

$$\gamma = \frac{m_{\text{surfactant}}}{m_{\text{water}} + m_{oil} + m_{\text{surfactant}}}. \qquad \text{Eq. 2-2.}$$

Note that it is also common to use volume fractions in order to describe the composition of the sample.

10

An extended three phase region can be found at low γ-values and intermediate temperatures. At temperatures below and above the three phase region the two different two phase regions $\underline{2}$ and $\overline{2}$ occur. The three-phase region meets the one-phase region at the so-called optimum point $\tilde{X}$ at which the microemulsion is at the optimum state [99] or balanced (from an HLB point of view) [108, 109]. This point is correlated to the optimum temperature $\tilde{T}$, at which the surfactant has the highest solubilisation properties, and the lowest surfactant mass fraction $\tilde{\gamma}$ with which it is possible to formulate a one-phase microemulsion. As $\tilde{\gamma}$ is used to characterise the efficiency of the surfactants in the system under investigation, $\tilde{X}$ is also called the efficiency point.

As microemulsion changes from oil-in-water to water-in-oil at the temperature $\tilde{T}$, this temperature is also called *phase inversion temperature* (PIT) [110, 111]. The phase inversion is founded in the change of solubility of the surfactant. Increasing temperature leads to weaker hydrogen bonds due to more molecular erratic movement [105].

The optimum state is a unique feature for every individual microemulsion composition. The location of the $\tilde{X}$-point is influenced by the hydrophobicity of the oil as well as by the amphiphilic properties of the surfactant. As can be seen in Figure 2.4 left, increasing the hydrophobic chain length from $i = 6$ to 12, the solubilisation efficiency of the surfactant increases. Furthermore, the higher hydrophobicity leads to a decrease of T_m so that lower temperatures are needed to change the solubility of the surfactant from water-soluble to hydrophobic. On the other hand, an increase of the hydrophilic chain length by varying the number of ethoxy units j between 2 and 7, leads to an increase of T_m which is accompanied by a slight decrease of γ_m.
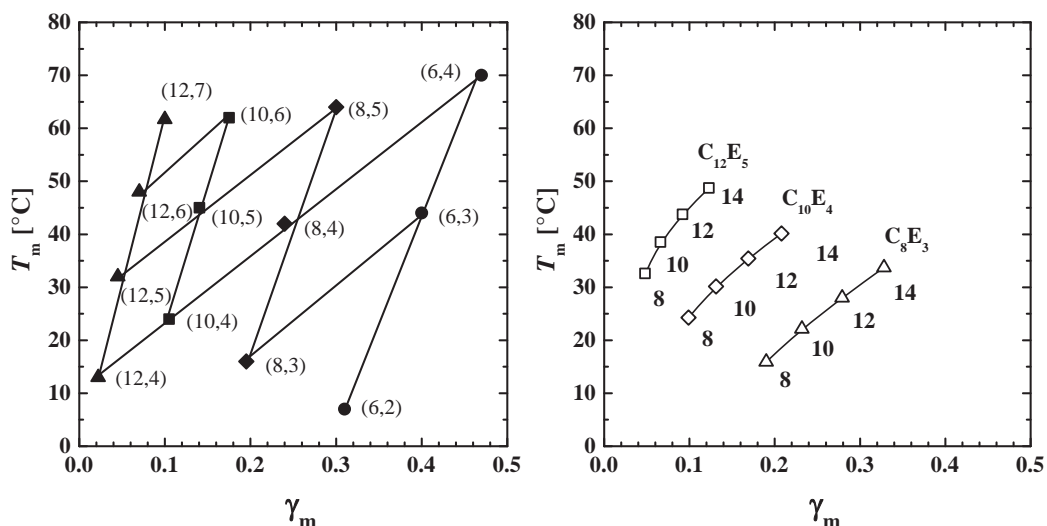

Figure 2.4: *Left:* X_m points of various H_2O – *n*-octane – C_iE_j microemulsions with equal volumes of water and octane as a function of the mean temperature T_m and the surfactant mass fraction γ_m [106]. The numbers in brackets indicate the chain length of the hydrophobic part i and the number of ethoxy units j in the hydrophilic chain in the form of (i, j). *Right:* Influence of alkanes (C_nH_{2n+2}) with different chain lengths on the X_m point in various microemulsions H_2O – alkane - C_iE_j [106]. For all three surfactants, an increase of the chain length of the alkane leads to a shift of the X_m point to higher temperatures T_m and surfactant mass fractions γ_m.

11

Figure 2.4 right illustrates the influence of the chain length of the hydrophobic component. Increasing the length of the alkane (which is indicated by the numbers below the points) leads to a shift of the X_m point to higher temperatures as well as to higher surfactant mass fractions γ_m. This is mainly due to the fact that longer oils are harder to solubilise. Since the lower miscibility gap within the binary system B-C shifts to higher temperatures with increasing alkane chain length higher temperatures are necessary to drive the surfactant from the water to the oil phase. A similar effect can also be seen for the binary mixture of alkane and surfactant [112].

In contrast to the $T(\gamma)$-section, the ratio γ_a

$$\gamma_a = \frac{m_C}{m_A + m_C} \qquad\qquad \text{Eq. 2-3}$$

of surfactant in the water-surfactant mixture is kept at a constant value in a $T(w_B)$-section (Figure 2.3 right). Here, the mass fraction of oil is varied. Accordingly, the composition of the sample is given by the mass fraction

$$w_B = \frac{m_B}{m_A + m_B + m_C} \qquad\qquad \text{Eq. 2-4}$$

of oil (m_B) in the overall mixture. At low w_B the whole amount of oil can be solubilised by the water-surfactant mixture and the one-phase region stretches over a wide range of temperature. At higher oil mass fractions, the two different two-phase regions also occur, whereby the phase sequence is similar to the one already mentioned for $T(\gamma)$ sections. The point of maximum efficiency here is $w_{B,max}$ at T_l and characterises the maximum amount of oil which can be solubilised by the given water-surfactant mixture. The lower phase boundary which separates the one-phase microemulsion from the 2̲ state is called oil emulsification failure boundary (*oefb*) [113, 114]. The upper phase boundary very often runs through a minimum at low w_B which is caused by the miscibility gap of the binary mixture water-surfactant for surfactants with high amphiphilic strength [98, 115]. Because of its proximity to the critical point of the binary mixture the upper phase boundary is also called the near critical boundary (*ncb*). In this case, a closed loop miscibility gap causes an unstable microemulsion which separates. The reasons for this closed loop are discussed in the following chapter.

2.1.3 Curvature of the amphiphilic film and microstructure

The most crucial point to predict the phase behaviour is the nature of the surfactant. Depending on the strength of its interactions with the hydrophilic and the hydrophobic phase a local curvature of the amphiphilic film develops [98]. Starting from the two principle radii R_1 and R_2 the curvatures c_i can be described by

$$c_1 = \frac{1}{R_1} \qquad \text{and} \qquad c_2 = \frac{1}{R_2} \qquad\qquad \text{Eq. 2-5}$$

12

Figure 2.5 shows three examples of different structures and the according radii.
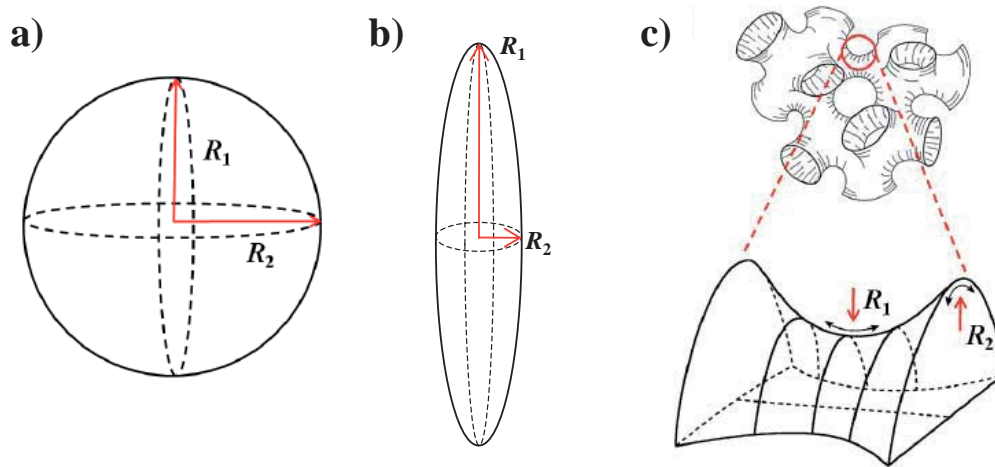

Figure 2.5: Principal curvature of a spherical (a) and a cylindrical (b) membrane and the membrane in a sponge structure, together with the curvature radii R_i. Redrawn and extended from [116].

For a spherical structure (Figure 2.5 a), the radii R_1 and R_2 are the same. Thus, it follows that $c_1 = c_2 = 1/R$. For a cylindrical structure as indicated by Figure 2.5 b) one radius is much larger than the other one. Figure 2.5 c) depicts a sponge-like structure with two different curvature radii, where R_1 describes the radius of the channel and R_2 represents the curvature of the channel itself.

Based on the parameters c_i it is also possible to define the mean curvature H

$$H = \tfrac{1}{2}(c_1 + c_2).$$

Eq. 2-6

The structures shown in Figure 2.5 and many more occur in microemulsions depending on composition and temperature. The mean curvature in microemulsions with non-ionic surfactants is mainly a function of temperature as a tuning parameter [98, 99] which is shown graphically in Figure 2.6 left by means of the so-called wedge model [117]. Here, a surfactant is represented by a wedge consisting of two parts and the strength of the interaction is represented by the volume (or area in a 2D plot) of the according part of the surfactant wedge. Thus, at low temperature the interactions between the surfactant head group and water outweigh the ones of surfactant and oil, which is why the hydrophilic part of the wedge requires a bigger volume than the hydrophobic part, leading to a curvature of the amphiphilic film around the oil ($H > 0$). At intermediate temperature the surfactant interacts both with water and oil, the parts of the wedge have the same value and the mean curvature is zero. Increasing the temperature further the interactions of oil and the hydrophobic part of the surfactant overbalance the ones of water and the hydrophilic part of the surfactant, thus leading to an amphiphilic film which is curved around water. This state is indicated by a negative value of H. The relation between morphology of the microstructure and the temperature-dependent mean curvature has experimentally been studied by means of conductivity and NMR-self diffusion measurements [98,

13

118-123], electron microscope imaging [124-126] as well as light, X-ray and neutron scattering [123, 127-141].
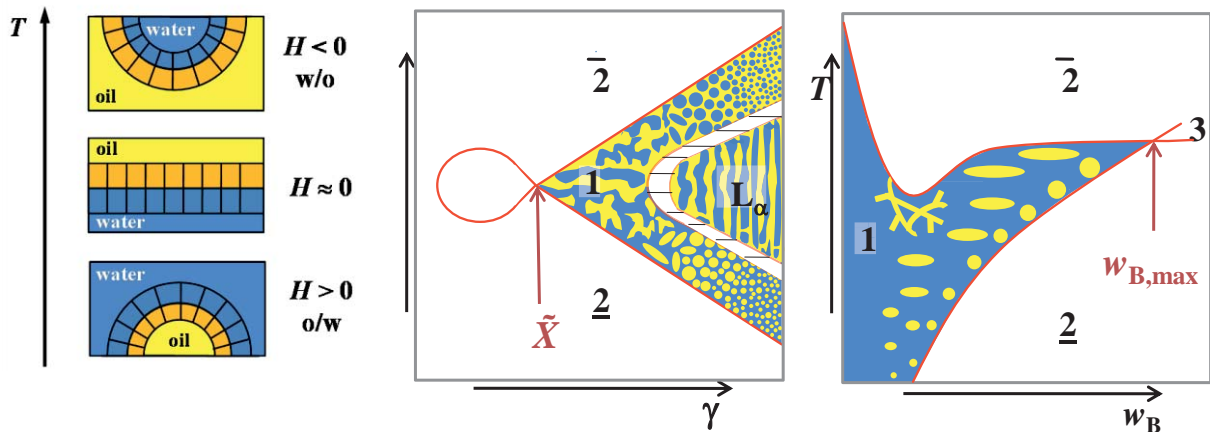

Figure 2.6: Schematic drawing of the mean curvature of the amphiphilic film as a function of temperature (left). Redrawn from [99]. This trend of the curvature can also be found in the different sections through the phase prism, the $T(\gamma)$-section (middle, redrawn according to [98]) and the $T(w_B)$-section (right), although the structures in the one-phase microemulsion differ considerably among these sections.

While the mean curvature of the amphiphilic film is mainly a function of temperature, the global structure also highly depends on the composition of the sample. For a microemulsion with a balanced ratio of oil and water, depicted in a $T(\gamma)$-section in Figure 2.6, the structure of the microemulsion close to the efficiency point is of bicontinuous nature [98]. By increasing the concentration of surfactant γ more interfacial area can be covered and thus the characteristic size decreases, leading to elongated structures and finally to spherical micelles at high surfactant concentration. At temperatures lower than $\tilde{T}$ oil-in-water structures can be found and at higher temperatures water-in-oil structures are present, following the trend of the curvature of the amphiphilic film in Figure 2.6 left.

In diluted microemulsion systems, as shown in Figure 2.6 right, spherical micelles can be found along the oil emulsification failure boundary [121]. Keeping the composition constant and increasing the temperature an elongation of the spherical micelles can be observed. The amphiphilic film at low temperature is, as shown in Figure 2.6 left, curved around the oil. By increasing the temperature the curvature of the film slowly approaches zero, leading to a flat amphiphilic film. In terms of microstructure, this effect becomes visible by the development of cylindrical structures where the curvature in the direction of the length is zero. Only the half-sphere shaped cylinder end caps have a high energy at this state. To avoid these high-energy parts the cylindrical micelles eventually form networks with Y-like junctions where the mean curvature of the amphiphilic film further approximates zero. If the minimum of the upper phase boundary is reached, given the according composition of the microemulsion, the microemulsion separates into two different phases, one concentrated and one diluted network structure. This can be explained by the number density of the network junctions which increases upon the connection of formerly independent cylinders. These junctions enable a certain

attraction of different oil domains which lead to the separation into two network phases with different concentrations of network structures. A mean curvature of $H = 0$ can be found in form of lamellar phases (L_α) at even higher temperatures.

By increasing the amount of oil in the microemulsion, i.e. increasing w_B, an oil-in-water microemulsion coexists with an oil excess phase at low temperature. Since the amount of oil in the microemulsion is low compared to the amount of water, the volume of the oil excess phase is very small. Upon increasing the temperature above the close proximity to the *oefb* the elongation to cylindrical micelles can also be observed at high w_B. Before the connection to networks happens, however, the microemulsion separates into a water-in-oil microemulsion and a water excess phase since the upper phase boundary is commonly at temperatures below the phase inversion temperature. Considering the volume ratios it becomes obvious that the microemulsion phase must be much smaller in volume than the water excess phase. Note that the three-phase region in a diluted microemulsion occurs at higher temperatures than the one of the point of maximum efficiency.

15